J|A|C|S
ARTICLES
Published on Web 01/26/2007

Structure and Dynamics of Surfactin Studied by NMR in Micellar Media

Pascale Tsan,*,‡ Laurent Volpon,‡ Françoise Besson,§ and Jean-Marc Lancelin*,‡

Contribution from the Université Claude Bernard - Lyon 1, Sciences Analytiques ANABIO, CNRS UMR 5180, Bâtiment CPE-Lyon, Domaine Scientifique de la Doua, F-69622 Villeurbanne, France, and Université Claude Bernard - Lyon 1, Laboratoire Organisation et Dynamique des Membranes Biologiques, CNRS UMR 5013, 43 Boulevard du 11 Novembre 1918, F-69622 Villeurbanne, France

Received August 23, 2006; E-mail: pascale@hikari.cpe.fr; lancelin@hikari.cpe.fr

Abstract: The NMR structure of the cyclic lipopeptide surfactin from *Bacillus subtilis* was determined in sodium dodecyl sulfate (SDS) micellar solution. The two negatively charged side chains of surfactin form a polar head opposite to most hydrophobic side chains, accounting for its amphiphilic nature and its strong surfactant properties. Disorder was observed around the fatty acid chain, and ^{15}N relaxation studies were performed to investigate whether it originates from a dynamic phenomenon. A very large exchange contribution to transverse relaxation rate R_2 was effectively observed in this region, indicating slow conformational exchange. Temperature variation and Carr−Purcell−Meiboom−Gill (CPMG) delay variation relaxation studies provided an estimation of the apparent activation energy around 35−43 kJ·mol^{-1} and an exchange rate of about 200 ms^{-1} for this conformational exchange. ^{15}N relaxation parameters were also recorded in dodecylphosphocholine (DPC) micelles and DMSO. Similar chemical exchange around the fatty acid was found in DPC but not in DMSO, which demonstrates that this phenomenon only occurs in micellar media. Consequently, it may either reflect the disorder observed in our structures determined in SDS or originate from an interaction of the lipopeptide with the detergent, which would be qualitatively similar with an anionic (SDS) or a zwitterionic (DPC) detergent. These structural and dynamics results on surfactin are the first NMR characterization of a lipopeptide incorporated in micelles. Moreover, they provide a model of surfactin determined in a more biomimetic environment than an organic solvent, which could be useful for understanding the molecular mechanism of its biological activity.

1. Introduction

Surfactin, a very powerful biosurfactant produced by various strains of *Bacillus subtilis*, is a cyclic heptapeptide closed by a β-hydroxy fatty acid and contains two acidic residues, Glu1 and Asp5 (Figure 1). Although its primary structure was elucidated about 40 years ago,[1] surfactin is still a subject of intense research because of its environmental applications as a biosurfactant and its potential applications in biomedical sciences.[2,3] A structural model of this peptide has been determined by NMR in DMSO.[4] Two conformations, *S1* and *S2*, have actually been found. Both display a saddle-shaped conformation, where the two charged side chains are gathered on the same side. They form a "claw" and provide a polar head opposite to a hydrophobic domain. The presence of at least two conformers for surfactin had been also suggested by FTIR and CD spectroscopy measurements.[5]

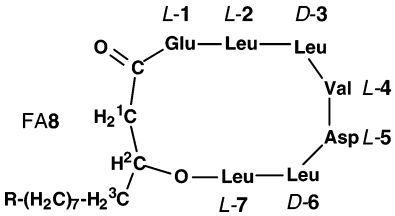

Figure 1. Primary structure of surfactin. *L*/*D* refers to the configuration of the amino acid. R = CH_3-$(CH_2)_2$-, CH_3-$CH(CH_3)$-, CH_3-$(CH_2)_3$, CH_3-$CH(CH_3)$-CH_2-, or CH_3-CH_2-$CH(CH_3)$- for the *n*C_{14}, *iso*C_{14}, *n*C_{15}, *iso*C_{15}, and *anteiso*C_{15} β-hydroxylated fatty acid 8, respectively.

The two NMR-evidenced structures could therefore explain the amphiphilic character of the molecule. Indeed, surfactin exhibits numerous biological activities, which presumably result from the interaction of this amphiphilic peptide with its target membrane. Thus, some experimental studies were carried out with biomimetic membranes such as vesicles[6,7] or lipid monolayers[8,9] to evaluate these effects. Several hypotheses on the

‡ Sciences Analytiques ANABIO, CNRS UMR 5180.
§ Laboratoire Organisation et Dynamique des Membranes Biologiques, CNRS UMR 5013.

(1) Kakinuma, A.; Hori, M.; Isono, M.; Tamura, G.; Arima, K. *Agric. Biol. Chem.* **1969**, *33*, 973−976.
(2) Mulligan, C. N. *Environ. Pollut.* **2005**, *133*, 183−198.
(3) Singh, P.; Cameotra, S. S. *Trends Biotechnol.* **2004**, *22*, 142−146.
(4) Bonmatin, J. M.; Genest, M.; Labbé, H.; Ptak, M. *Biopolymers* **1994**, *34*, 975−986.
(5) Vass, E.; Besson, F.; Majer, Z.; Volpon, L.; Hollosi, M. *Biochem. Biophys. Res. Commun.* **2001**, *282*, 361−367.
(6) Carrillo, C.; Teruel, J. A.; Aranda, F. J.; Ortiz, A. *Biochim. Biophys. Acta* **2003**, *1611*, 91−97.
(7) Heerklotz, H.; Seelig, J. *Biophys. J.* **2001**, *81*, 1547−1554.
(8) Maget-Dana, R.; Ptak, M. *Biophys. J.* **1995**, *68*, 1937−1943.
(9) Deleu, M.; Nott, K.; Brasseur, R.; Jacques, P.; Thonart, P.; Dufrene, Y. F. *Biochim. Biophys. Acta* **2001**, *1513*, 55−62.

10.1021/ja066117q CCC: $37.00

mode of action of surfactin are proposed, such as membrane permeabilization,[6,10] membrane disruption by detergent effect,[7] complexation of ions and transport across the membrane,[11] and modification of the membrane physical properties.[12]

Additional studies by computer simulations provided a picture at the molecular level of the conformation[13,14] or some dynamic properties[15] of surfactin in interaction with a membrane-mimicking environment. As the three-dimensional (3-D) structure of the peptide was required for their modeling, these studies used the *S1* and *S2* structures of surfactin determined in DMSO and obtained slightly different results between the two families. In modeling surfactin at a hydrophobic/hydrophilic interface, Gallet et al.[14] found that the *S2* conformation with a folded fatty chain was the conformation that gave the most consistent interfacial characteristics compared with those obtained experimentally by a Langmuir film balance. Deleu et al.[13] simulated the interaction of surfactin with membranes and found that *S1* and *S2* structures were inserted differently into the membranes. For *S2*, the two acidic residues are located in the polar head region whether the membrane is charged or uncharged. In contrast, for *S1*, Asp5 happens to protude in the aqueous medium in charged membranes, while Glu1 is found in the hydrophobic core in uncharged membranes. The authors did not exclude the possibility of a reversible transition between the two conformers during the penetration and the spanning of surfactin in the membrane, and they suggested that *S2* might correspond to a calcium-bound surfactin while *S1* would correspond to the cation-free lipopeptide. Finally, molecular dynamics simulation at a water−hexane interface suggested that *S2* 3-D conformation is not conserved at any lateral pressure while *S1* 3-D conformation is conserved at high lateral pressure.[15] The mode of interaction of surfactin with membranes is therefore still unclear and seems to depend not only on the model of membrane used but also on the choice between the *S1* or *S2* structure.

Since the biological role of surfactin had been explained mainly by its affinity for cell membranes, it is particularly important to study its interaction with amphiphilic molecules that might mimick the environment of surfactin incorporated into biological membranes better than a water−hexane interface. Among these amphiphilic molecules, the most common membrane-mimicking aqueous media compatible with NMR studies in solution are detergents such as sodium dodecyl sulfate (SDS) and dodecyl phosphocholine (DPC). DPC in particular contains a polar phosphocholine head as some glycero- and sphingophospholipids, the major natural components of biological membranes. SDS and DPC can solubilize membrane proteins or lipopeptides and form micelles of about 60 molecules,[16,17] which generally give a short enough correlation time for NMR studies in liquids. This led us to study surfactin in a SDS or DPC solution using NMR spectroscopy and to thoroughly investigate its dynamics properties in this environment.

Numerous polypeptide structures have been determined in micelles, fewer have investigated in details the dynamic properties. Moreover, they concern larger peptides mainly constituted of amphiphilic helices. The smallest peptides for which detailed relaxation studies in micelles have been reported are helical peptides such as the 25-residue pleurocidin,[18] the 30 N-terminal residues of HIV-1 gp41,[19] and the 36-residue neuropeptide Y.[20] No detailed NMR dynamics data have been reported, to our knowledge, for lipocyclopeptides in micelles.

^{15}N Uniform labeling of surfactin enabled us to investigate in detail its dynamic properties in negatively charged SDS micelles, using the longitudinal (R_1) and the transverse (R_2) ^{15}N relaxation rates and the heteronuclear ^{1}H−^{15}N NOE measured at several temperatures and with various CPMG delays for the R_2 experiments. These results were then complemented by relaxation measurements in DPC uncharged micelles and in DMSO. Therefore, this affords an evaluation of the effect of the various solvents on surfactin, both from structural and dynamic points of view.

2. Experimental Section

2.1. Lipopeptide Production. ^{15}N-Labeled surfactin was extracted from *Bacillus subtilis*, grown in the same $^{15}NH_4Cl$-containing medium as that in ref 21, and purified according to ref 5.

2.2. NMR Experiments. Two milligrams of surfactin was dissolved in aqueous (90% H_2O, 10% D_2O) micellar solutions of 15−150 mM SDS-d_{25} (Euriso-top), and the pH was adjusted to 5.1. Surfactin samples of similar concentration were prepared with DPC (Avanti Polar Lipids) at 70 mM, pH 6.0, and in DMSO-d_6 (Aldrich). All NMR spectra were recorded on a Bruker Avance DRX 500 spectrometer using a 5-mm (^{1}H,^{13}C,^{15}N) triple-resonance probe head, equipped with a supplementary self-shielded *z*-gradient coil. Homonuclear 2-D spectra DQF-COSY,[22] TOCSY (HOHAHA),[23,24] and NOESY[25,26] were recorded in the phase-sensitive mode using the States-TPPI method[27] as data matrices of 512 real (t_1) × 1024 (t_2) complex data points; 32 scans per t_1 increment with 1.5 s recovery delay and spectral width of 5734 Hz in both dimensions were used. The mixing times were 80 ms for TOCSY and 100, 150, 250, and 400 ms for the NOESY experiments. Spectra were processed using GIFA V.4[28] software with shifted sine-bell and Gaussian window apodization functions in both F_1 and F_2 dimensions after zero-filling in the t_1 dimension to obtain a final matrix of 1024 (F_1) real × 1024 (F_2) complex data points. Chemical shifts were referenced to the solvent chemical shifts.

^{15}N HSQC[29] were recorded using the echo−antiecho method[30] with 180 (t_1, ^{15}N) and 1024 (t_2, ^{1}H) complex points and 24 scans per t_1 increment. R_1 and R_2 ^{15}N relaxation rates as well as the steady-state ^{1}H−^{15}N heteronuclear NOE measurements were performed using the

(10) Sheppard, J. D.; Jumarie, C.; Cooper, D. G.; Laprade, R. *Biochim. Biophys. Acta* **1991**, *1064*, 13−23.
(11) Thimon, L.; Peypoux, F.; Wallach, J.; Michel, G. *Colloids Surf. B* **1993**, *1*, 57−62.
(12) Epand, R. M. *Biopolymers* **1997**, *43*, 15−24.
(13) Deleu, M.; Bouffiouw, O.; Razafindralambo, H.; Paquot, M.; Hbid, C.; Thonart, P.; Jacques, P.; Brasseur, R. *Langmuir* **2003**, *19*, 3377−3385.
(14) Gallet, X.; Deleu, M., Razafindralambo, H., Jacques, P., Thonart, P., Paquot, M.; Brasseur, R. *Langmuir* **1999**, *15*, 2409−2413.
(15) Nicolas, J. P. *Biophys. J.* **2003**, *85*, 1377−1391.
(16) Mysels, K.; Princen, L. *J. Phys. Chem.* **1959**, *63*, 1696−1700.
(17) Lauterwein, J.; Bosch, C.; Brown, L. R.; Wüthrich, K. *Biochim. Biophys. Acta* **1979**, *556*, 244−264.
(18) Syvitski, R. T.; Burton, I.; Mattatall, N. R.; Douglas, S. E.; Jakeman, D. L. *Biochemistry* **2005**, *44*, 7282−7293.
(19) Jaroniec, C. P.; Kaufman, J. D.; Stahl, S. J.; Viard, M.; Blumenthal, R.; Wingfield, P. T.; Bax, A. *Biochemistry* **2005**, *44*, 16167−16180.
(20) Bader, R.; Bettio, A.; Beck-Sickinger, A. G.; Zerbe, O. *J. Mol. Biol.* **2001**, *305*, 307−329.
(21) Volpon, L.; Besson, F.; Lancelin, J.-M. *FEBS Lett.* **2000**, *485*, 76−80.
(22) Rance, M.; Sorensen, O. W.; Bodenhausen, G.; Wagner, G.; Ernst, R. R.; Wüthrich, K. *Biochem. Biophys. Res. Commun.* **1983**, *117*, 479−485.
(23) Braunschweiler, L.; Ernst, R. R. *J. Magn. Reson.* **1983**, *53*, 521−528.
(24) Davies, D. G.; Bax, A. *J. Am. Chem. Soc.* **1985**, *107*, 2820−2821.
(25) Jeener, J.; Meier, B. H.; Bachmann, P.; Ernst, R. R. *J. Chem. Phys.* **1979**, *71*, 4546−4553.
(26) Macura, S.; Hyang, Y.; Suter, D.; Ernst, R. R. *J. Magn. Reson.* **1981**, *43*, 259−281.
(27) Marion, D.; Ikura, M.; Tschudin, R.; Bax, A. *J. Magn. Reson.* **1989**, *85*, 393−399.
(28) Pons, J. L.; Malliavin, T. E.; Delsuc, M. A. *J. Biomol. NMR* **1996**, *8*, 445−452.
(29) Bodenhausen, G.; Ruben, D. J. *Chem. Phys. Lett.* **1980**, *69*, 185−189.
(30) Bachmann, P.; Aue, W. P.; Muller, L.; Ernst, R. R. *J. Magn. Reson* **1977**, *28*, 29−39.

usual pulse sequences.[31] The R_1 and R_2 experiments were collected with 80 complex t_1 increments, 1024 t_2 points, and 40 scans for each FID. For R_1 measurements, spectra were recorded with seven inversion recovery delays of 22, 55, 155 (×2), 255, 500, 755, and 1100 ms. For R_2 measurements, spectra were recorded at seven CPMG delays of 17, 33, 50 (×2), 67, 83, 100, and 133 ms. The delay between two 180° ^{15}N pulses in the CPMG sequence was set to 900 μs for all experiments unless stated otherwise (CPMG delay variation study at 380, 120, and 68 μs as well). ^{1}H−^{15}N NOE spectra with 60 × 2 complex t_1 increments, 1024 t_2 points, and 128 scans per FID were recorded in an interleaved way with and without proton saturation during relaxation delay. Recycle delays of 5 and 2 s were used for the spectra recorded respectively in the absence and in the occurrence of proton saturation. The ^{15}N saturation was achieved by the application of 120° ^{15}N pulses separated by 5 ms, for a period of 3 s. Spectral widths for all heteronuclear experiments were 3005 Hz in F_1 and 1216 Hz in F_2 with carrier frequencies at 122 and 8.5 ppm, respectively. Data were processed using PIPP software.[32] They were apodized with a shifted square sine-bell window in both dimensions, after zero-filling in the t_1 dimension to obtain a final matrix of 128 (F_1) × 1024 (F_2) real data points.

2.3. Structure Calculations. Interproton-distance restraints were derived from homonuclear NOESY experiments and classified into three categories. Upper bounds were fixed at 2.7, 3.3, and 5.0 Å for strong, medium, and weak correlations, respectively. The intensity of the NOE between a methylene pair was used as a reference for a distance of 1.8 Å; 0.3 Å were added to NOEs involving amide or hydroxy protons. Pseudo-atom corrections[33] of the upper bounds were applied for distance restraints involving the unresolved methyl or methylene protons (+1 Å). For nonstereospecifically assigned but spectroscopically resolved diastereotopic protons, the interproton distances were treated as single $(\langle r^{-6}\rangle)^{-1/6}$ average distances. The lower bound for all restraints was fixed at 1.8 Å, which corresponds to the sum of the hydrogen van der Waals' radii. Dihedral angle restraints χ_1 were deduced from the stereospecific assignments of diastereotopic β-protons.[34,35] Models were calculated following protocols as previously described[35] using the X-PLOR software version 3.851.[36] The structures and the simple charge potentials associated to solvent-accessible surfaces were visualized using the MOLMOL version 2.4.[37]

2.4. Relaxation Data Analysis. Peak heights of the ^{15}N−^{1}H cross-peaks were measured using PIPP software, and the uncertainty was estimated by NmrPipe.[32] The cross-peak heights were then fit to a single-exponential decay function $I(t) = I_0\, e^{-Rt}$ to get the R_1 and R_2 values ($I(t)$ is the intensity at relaxation delay t, I_0 the intensity at $t = 0$). The errors in R_1 or R_2 were estimated by Monte Carlo simulations. The ^{1}H−^{15}N heteronuclear NOE was calculated from the ratio between the intensities of a peak in the spectra collected with and without proton saturation, respectively. The errors in the NOE values were determined as standard errors.

The spectral density function values can be obtained at three frequencies from R_1, R_2, and NOE measurement, using the following equations:[38−41]

$$J_{eff}(0) = 3[-R_1/2 + R_2 - (3/5)R_{NOE}]/2(3d^2+c^2) \quad (1)$$

$$J(\omega_N) = [R_1 - (7/5)R_{NOE}]/(3d^2+c^2) \quad (2)$$

$$\langle J(\omega_H)\rangle = R_{NOE}/5d^2 \quad (3)$$

where $R_{NOE} = R_1$ (NOE − 1) (γ_N/γ_H), $d^2 = (\mu_0/4\pi)^2\gamma_H^2\gamma_N^2h^2/(16\pi^2\langle 1/r^3\rangle^2)$, $c^2 = \gamma_N^2B_0^2\Delta^2/3$, μ_0 is the permeability in vacuum, γ_H and γ_N the magnetogyric ratios for ^{1}H and ^{15}N, h Planck's constant, B_0 the magnetic field strength, Δ the chemical shift anisotropy estimated at −160 ppm,[42] and r the NH bond length taken as 1.02 Å. $J_{eff}(0)$ denotes that exchange contribution to R_2 is not explicitly considered.[43] $\langle J(\omega_H)\rangle$ is the average of $J(\omega_H)$, $J(\omega_H + \omega_N)$, and $J(\omega_H - \omega_N)$ that can be approximated by $J(0.87\omega_H)$.[38]

Tensor[44] was used for the Lipari−Szabo analysis[45,46] of the relaxation parameters. The following models were iteratively tested, until the model fits the measured relaxation rates within 95% confidence limits: model 1 (order parameter S^2), model 2 (S^2, internal correlation time τ_i), model 3 (S^2, chemical exchange term R_{ex}), model 4 (S^2, τ_i, R_{ex}), model 5 (order parameter for the rapid librational motion S_f^2, order parameter for the slow internal motion S_s^2, τ_i).

Considering a chemical exchange between two sites, the contribution of the exchange term R_{ex} to R_2 can be approximated, in the limit of fast exchange, by:

$$R_{ex} = \left[\frac{p_A p_B(\Delta\omega)^2}{k_{ex}}\right]\cdot\left[1 - \left(\frac{2}{k_{ex}\tau_{CPMG}}\right)\tanh\left(\frac{k_{ex}\tau_{CPMG}}{2}\right)\right] \quad (4)$$

where τ_{CPMG} is the delay between 180° pulses in the CPMG pulse train used for the R_2 experiment, $\Delta\omega$ is the difference of chemical shift in the two conformational states, p_A and p_B are the populations in the two conformational states, and k_{ex} is the apparent exchange rate constant.[47]

According to Mandel et al., [48] the slope of $\ln(R_{ex})$ versus $1/T$ provides an estimate of the apparent activation energy between the two conformational states. Actually, these values can be slightly underestimated, but by less than a factor of 2.[48]

The temperature dependence of the order parameter can be related to a parameter T^* defining a characteristic temperature for the dynamical process. T^*/T indeed reflects the density of energy states thermally accessible to the bond vector.[48]

$$\frac{d(1-S)}{dT} = \frac{3}{2T^*} \quad (5)$$

3. Results

3.1. Structural Studies in SDS Solution. 3.1.1. Effects of the SDS Concentration and Assignment. In order to characterize surfactin in more biomimetic conditions than an organic solvent, the lipopeptide was studied in aqueous solution supplemented by SDS detergent to remedy its very low solubility.[49] 1D spectra of surfactin at a concentration around 4 mM were recorded at 25 °C with increasing SDS concentrations (15, 30, 50, 70, and 150 mM). Up to 50 mM SDS, slight

(31) Farrow, N. A.; Muhandiram, R.; Singer, A. U.; Pascal, S. M.; Kay, C. M.; Gish, G.; Shoelson, S. E.; Pawson, T.; Forman-Kay, J. D.; Kay, L. E. *Biochemistry* **1994**, *33*, 5984−6003.
(32) Garrett, D. S.; Powers, R.; Gronenborn, A. M.; Clore, G. M. *J. Magn. Reson.* **1991**, *95*, 214−220.
(33) Wüthrich, K. *NMR of Proteins and Nucleic Acids*; Wiley-Interscience: New York, 1986.
(34) Hyberts, S. G.; Marki, W.; Wagner, G. *Eur. J. Biochem.* **1987**, *164*, 625−635.
(35) Wagner, G.; Braun, W.; Havel, T. F.; Schaumann, T.; Go, N.; Wüthrich, K. *J. Mol. Biol.* **1987**, *196*, 611−639.
(36) Brünger, A. T. *X-PLOR*, Version 3.851; Yale University Press: New Haven, CT, 1996.
(37) Koradi, R.; Billeter, M.; Wüthrich, K. *J. Mol. Graphics* **1996**, *14*, 51−55.
(38) Farrow, N. A.; Zhang, O.; Szabo, A.; Torchia, D. A.; Kay, L. E. *J. Biomol. NMR* **1995**, *6*, 153−162.
(39) Ishima, R.; Yamasaki, K.; Saito, M.; Nagayama, K. *J. Biomol. NMR* **1995**, *2*, 217−220.
(40) Ishima, R., Nagayama, K. *Biochemistry* **1995**, *34*, 3162−3171.
(41) Lefevre, J. F.; Dayie, K. T.; Peng, J. W.; Wagner, G. *Biochemistry* **1996**, *35*, 2674−2686.
(42) Hiyama, Y.; Niu, C.; Silverton, J. V.; Bavoso, A.; Torchia, D. A. *J. Am. Chem. Soc.* **1988**, *110*, 2378−2383.
(43) Peng, J. W.; Wagner, G. *Biochemistry* **1995**, *34*, 16733−16752.
(44) Dosset, P.; Hus, J.-C.; Blackledge, M.; Marion, D. *J. Biomol. NMR* **2000**, *16*, 23−28.
(45) Lipari, G.; Szabo, A. *J. Am. Chem. Soc.* **1982**, *104*, 4546−4559.
(46) Lipari, G.; Szabo, A. *J. Am. Chem. Soc* **1982**, *104*, 4560−4570.
(47) Luz, Z.; Meiboom, S. *J. Chem. Phys* **1963**, *39*, 366−370.
(48) Mandel, A. M.; Akke, M.; Palmer, A. G., III. *Biochemistry* **1996**, *35*, 16009−16023.
(49) Thimon, L.; Peypoux, F.; Michel, G. *Biotechnol. Lett.* **1992**, *14*, 713−718.

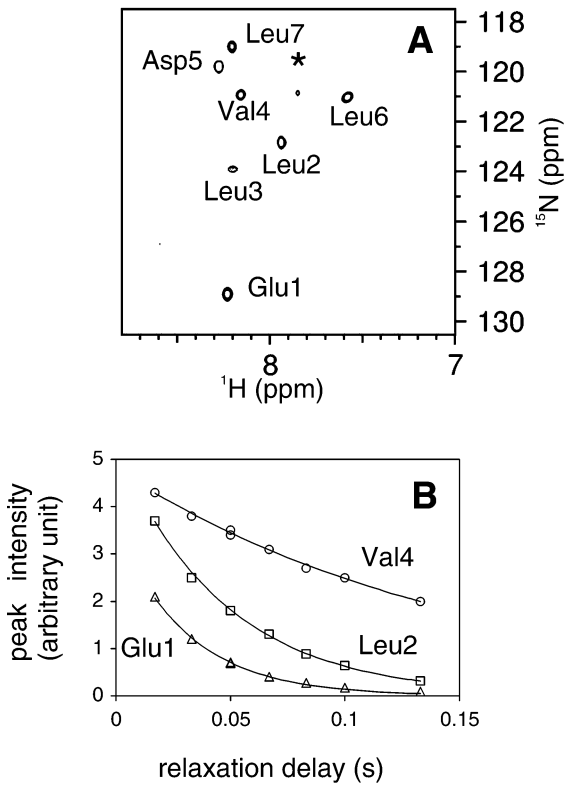

Figure 2. (A) ^{15}N HSQC spectrum and (B) R_2 relaxation curves for residues 1 (triangles), 2 (squares), and 4 (circles) of surfactin in SDS aqueous solution pH = 6.0 at 35 °C. The asterisk indicates a peak from impurity. R_2 experiment was duplicated at the relaxation delay of 0.05 s.

variations in chemical shift as well as line width narrowing could be observed. Then no change occurred at higher concentrations of SDS. The detergent concentration was therefore set around 50 mM for the further experiments, which corresponds to an approximately 4:1 peptide to micelle ratio. Proton and ^{15}N assignment (Supporting Information) was straightforward, using the standard COSY, TOCSY, NOESY, and ^{15}N HSQC experiment (Figure 2A).

3.1.2. Amide Proton Exchange Rates. Exchange rates of amide protons with solvent were evaluated following ^{15}N HSQC spectra of surfactin in SDS solution with D_2O, at 15 °C. We found that amide protons were exchanged after 10 min for Leu2, 20 min for Glu1, Val4 and Asp5, 30 min for Leu6, and 60 min for Leu3 and Leu7.

3.1.3. Structure Calculation. The surfactin structure was calculated using 47 intramolecular distance restraints: 6 intraresidual, 27 sequential $d(i, i + 1)$, and 14 short-range (9 $d(i, i + 2)$ and 5 $d(i, i + 3)$) distance restraints. Additionally, a NOESY experiment was recorded using a mixture of unlabeled SDS and fully deuterated SDS in a 1:3 ratio to attempt to find intermolecular NOE cross-peaks between surfactin and SDS. Unfortunately, none of these could be observed. Two χ_1 angle restraints were used as well: $+60° \pm 60°$ for Glu1 and $-60° \pm 60°$ for Asp5. Among the 50 structures generated by XPLOR using *allhdg.pro* forcefield, 24 were retained for structure refinement under CHARMM22 forcefield. The coordinates of the 24 final structures have been deposited in the Protein Data Bank (PDB entry 2NPV), and structural statistics are given in Table 1. The backbone RMSD is 0.50 Å, but as shown in Figure 3A, the Leu7 and FA8 region is relatively poorly defined, and the RMSD decreases to 0.30 Å if this region is ignored. The

Table 1. RMSD and Energy Statistics for the Ensemble of 24 Structures Obtained for Surfactin in SDS Solution at 25 °C

RMSD (Å)	
backbone atoms	0.50
heavy atoms	3.77
potential energies[a] (kcal·mol^{-1})	
F_{total}	-46.03 ± 6.52
F_{bond}	2.36 ± 0.22
F_{angle}	21.52 ± 2.34
F_{impr}	1.17 ± 0.46
$F_{Coulombic}$	-26.00 ± 3.66
F_{L-J}	-81.32 ± 3.13
F_{dihe}	35.46 ± 2.87
F_{noe}	0.77 ± 0.46
F_{cdih}	0.02 ± 0.02
average number of violations per structure	
NOE violations > 0.1 Å	0.84
dihedral violations > 5°	0

[a] F_{bond} is the bond-length deviation energy; F_{angle} is the valence angles deviation energy; F_{dihe} is the dihedral angles deviation energy; F_{impr} is the deviation energy for the improper angles used to maintain the planarity of certain groups of atoms; $F_{Coulombic}$ is the Coulombic energy contribution to the total energy F_{total}; F_{L-J} is the Lennard-Jones van der Waals energy function; F_{noe} is the experimental NOE function calculated using a force constant of 25 kcal·mol^{-1}·Å^{-2}; and F_{cdih} is the experimental function corresponding to the violations of the dihedral angle constraints.

two carboxylic groups of Glu5 and Asp1 are found to be at a distance of 4.3 ± 0.5 Å and form a negatively charged patch on the molecule surface (Figure 3, C and D). Finally, a few hydrogen bonds are observed on the lipopeptide backbone and form turns in most cases: $1H^N$-7CO (18 models out of 24), $4H^N$-1CO (19/24) (β turns of type II), and $5H^N$-1CO (23/24).

3.2. ^{15}N Relaxation in SDS Solution. 3.2.1. Relaxation Parameters. R_1, R_2, and heteronuclear ^{1}H−^{15}N NOE were measured for the seven backbone amides of surfactin in SDS solution at 15, 25, and 35 °C. As shown in Figure 4, R_1 and NOE do not vary much along the amino acid sequence. The averages for R_1 were 1.52 ± 0.18, 1.57 ± 0.11, and 1.70 ± 0.07 s^{-1}, and those for NOE were 0.44 ± 0.07, 0.31 ± 0.04, and 0.07 ± 0.04, respectively at 15, 25, and 35 °C (Table 2). In contrast, R_2 is dramatically high for Asp1, Leu2, and Leu7, compared to that for the other residues (see fitting curves in Figure 2B), and could not even be reliably determined at 15 °C for Asp1 due to an excessive signal broadening. The average values of R_2 calculated without those residues were 15.72 ± 0.52, 11.11 ± 2.18 , and 7.12 ± 1.26 s^{-1}.

3.2.2. Reduced Spectral Density Mapping. Reduced spectral density mapping, which does not require any hypothesis on the rotational diffusion tensor nor on the possibility to separate different time-scale motion was used first to analyze the relaxation data. $J_{eff}(0)$, $J(\omega_N)$, and $\langle J(\omega_H)\rangle$ spectral density values were calculated using eqs 1−3. As displayed in Figure 5, $J_{eff}(0)$ is particularly high for residues 1, 2, and 7, likely arising from a very large contribution of a μs−ms time-scale exchange contribution. As expected, $J(\omega_N)$ and $\langle J(\omega_H)\rangle$ values increase with temperature, whereas $J_{eff}(0)$ values decrease with temperature, due to the increase of the molecular tumbling rate and thus to the decrease of the global correlation time. $J(\omega_N)$ and $\langle J(\omega_H)\rangle$ high-frequency terms do not vary much among the seven amino acids, indicating similar motions on the fast time scale.

3.2.3. Model-Free Analysis. To obtain a more detailed picture of the dynamics of this small peptide in SDS micelles, we attempted a Lipari−Szabo analysis of this ensemble of data. The rotational diffusion tensor is usually characterized using

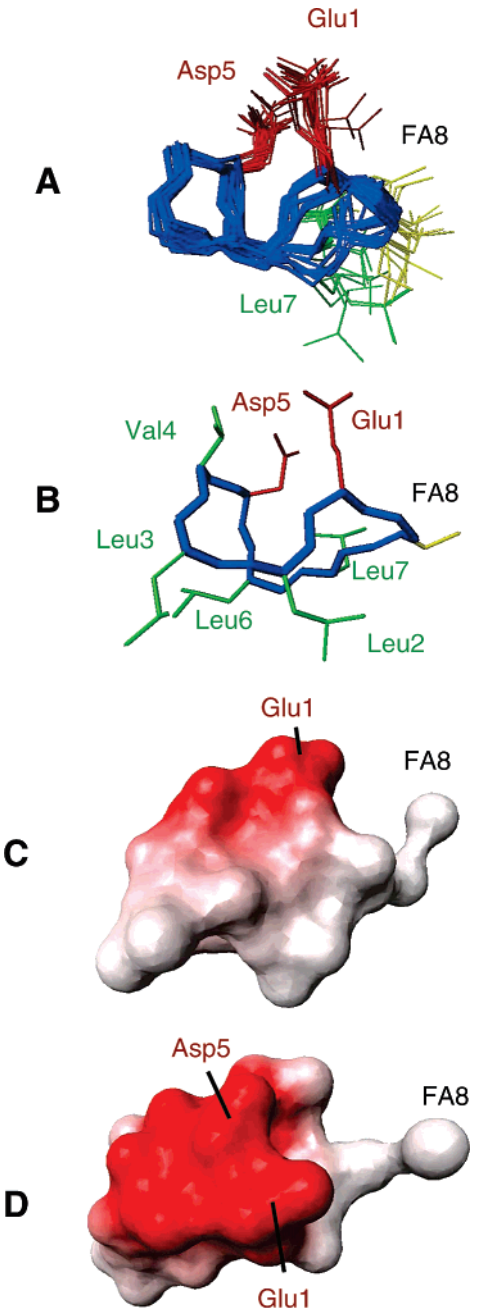

Figure 3. NMR structure of surfactin in SDS aqueous solution at 25 °C. (A) Superposition of the 24 structures and (B) representation of the closest structure to the geometric average. The superposition was performed using the backbone atoms of residues 1−6. For clarity, only heavy atoms are shown, and representation of the FA8 side chain is restricted to the C^3, C^4 carbons. The backbone is in blue, the two negatively charged side chains are in red, the FA8 fatty acid in yellow, and the other hydrophobic residues in green. For clarity, only the side chains of Asp5 and Glu1 as well as those of the disordered Leu7 and FA8 residues are represented in (A). (C) Electrostatic potentials associated to solvent-accessible surfaces for the closest structure to the geometric average. The negative charges present in the molecule are represented in red. In (C) the orientation is the same as that in (A) and (B), whereas (D) displays a top view.

R_2/R_1 ratio for residues displaying no internal dynamics on the fast time scale nor chemical exchange (model 1 with S^2 order parameter only).[50] These residues can be selected by two different methods. They can either be taken within known rigid secondary structures or be selected by the following two

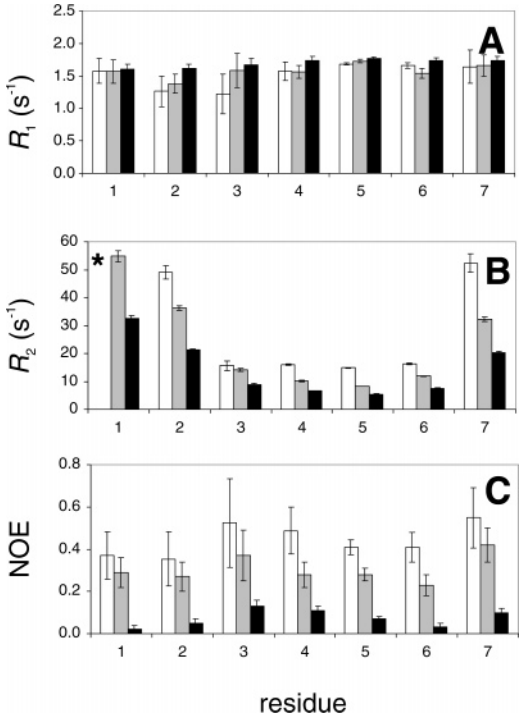

Figure 4. Backbone amide relaxation parameters at 11.7 T for surfactin in SDS aqueous solution. ^{15}N longitudinal (A) and transverse (B) relaxation rates and $^1H-^{15}N$ heteronuclear cross relaxation (C) were recorded at 15 °C (white boxes), 25 °C (gray boxes), and 35 °C (black boxes). The asterisk indicates that the R_2 value of residue 1 at 15 °C could not be reliably determined due to very fast relaxation.

Table 2. Average R_1, R_2, NOE, and Order Parameter Values for Surfactin in SDS, DPC, and DMSO Media

conditions	R_1 (s^{-1})	R_2 (s^{-1})[a]	NOE	$S^{2\,b}$
SDS (15 °C)	1.52 ± 0.18	15.72 ± 0.52	0.44 ± 0.07	0.86 ± 0.10
SDS (25 °C)	1.57 ± 0.11	11.11 ± 2.18	0.31 ± 0.04	0.67 ± 0.04
SDS (35 °C)	1.70 ± 0.07	7.12 ± 1.26	0.07 ± 0.04	0.59 ± 0.03
DPC (35 °C)	1.80 ± 0.14	10.91 ± 2.93	0.40 ± 0.10	-
DMSO (25 °C)	1.51 ± 0.08	12.15 ± 0.38	0.41 ± 0.05	-

[a]The average value was calculated excluding residues 1, 2, 7 for the data in SDS and DPC, and excluding residues 3 and 5 for the data in DMSO, as these R_2 values possess a very large contribution from chemical exchange. [b] S^2 was determined in SDS micelles only (see text).

criteria: (i) a high NOE value and (ii) a R_2/R_1 ratio that deviates by less than one standard deviation from the mean value.[51] Due to the absence of secondary structures in the lipopeptide, we had to choose the second method and used the data at 15 °C, for which the NOE values were still relatively high, excluding residues 1, 2, and 7 because of their high R_2/R_1 ratio. Given the very few data available due to the size of the peptide, we moreover assumed an isotropic tumbling. This hypothesis should be reasonable since this small peptide is solubilized and bound to SDS micelles that can be assimilated to spheres of about 60 molecules. Then the overall tumbling can simply be described by a single correlation time, for which a value of 10.9 ± 0.1ns was inferred by Tensor[44] from the R_2/R_1 ratios of residues 3−6. This value was then used to determine the local dynamics parameters. We found that only residue 3 could be rigorously modeled with model 1 (S^2) and therefore obeyed the assumptions required for a fair determination of τ_c. The others had to be

(50) Kay, L. E.; Torchia, D. A.; Bax, A. *Biochemistry* **1989**, *28*, 8972−8979.

(51) Clore, G. M.; Driscoll, P. C.; Wingfield, P. T.; Gronenborn, A. M. *Biochemistry* **1990**, *29*, 7387−7401.

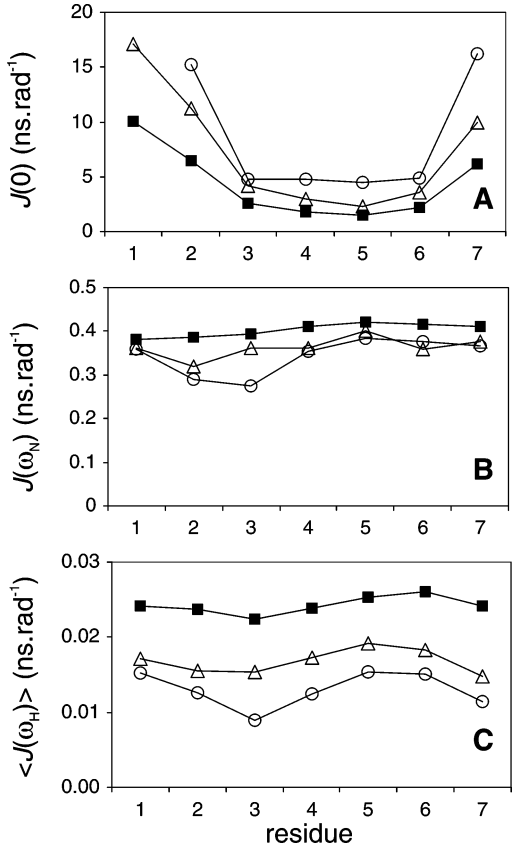

Figure 5. Spectral density function values for surfactin in SDS aqueous solution. (A) $J_{eff}(0)$, (B) $J(\omega_N)$, and (C) $\langle J(\omega_H)\rangle$ values were obtained at 15 °C (circles), 25 °C (triangles) and 35 °C (filled squares). The $J_{eff}(0)$ value of residue 1 at 15 °C could not be determined due to missing R_2 value.

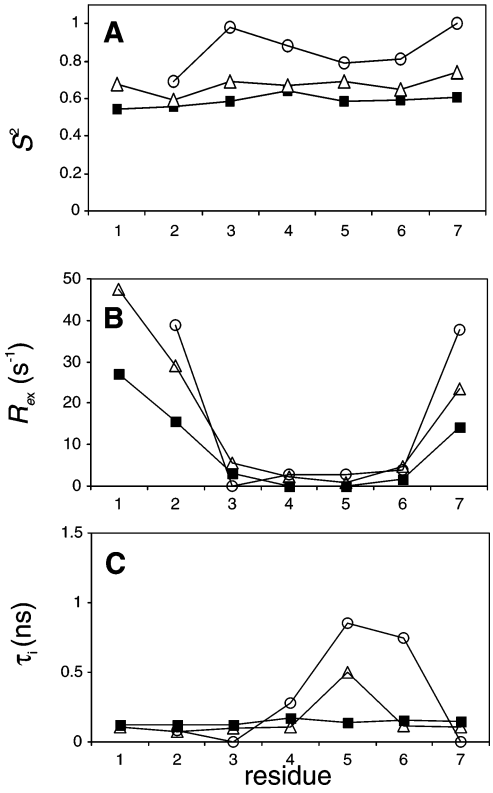

Figure 6. Dynamical parameters from a model-free analysis for surfactin in SDS micelles. (A) Order parameters, (B) exchange terms, and (C) internal correlation times are plotted versus residue number at 15 °C (circles), 25 °C (triangles), and 35 °C (filled squares). Values of residue 1 at 15 °C could not be determined due to missing R_2 value.

modeled with model 3 (S^2, R_{ex}) or model 4 (S^2, R_{ex} τ_i) by Tensor, using, however, small values of R_{ex} and τ_i. We then selected only residue 3 to derive τ_c and found exactly the same value. As a consequence, the previous mobility parameters calculated with $\tau_c = 10.9$ ns were kept. Because of the very low NOE values for all residues at 25 and 35 °C, we estimated the correlation time at those temperature from the time determined at 15 °C, using the Stokes−Einstein equation $\tau_c = V\eta/kT$, where V is the volume of the molecule, η the viscosity of the solution, and k the Boltzmann constant. Thus, taking the values of water viscosity η =1.139, 0.891, and 0.720 mPa·s at 15, 25, and 35 °C respectively, we estimated that $\tau_c = 8.2 \pm 0.1$ ns at 25 °C and 6.4 ± 0.1 ns at 35 °C. Local mobility parameters were therefore derived using these different τ_c values, and results are presented in Figure 6 for each temperature. One can notice that the order parameter does not vary much along the peptide sequence and globally decreases with temperature. Average values are 0.85, 0.67, and 0.58 at 15, 25, and 35 °C, respectively, showing an increase of the backbone flexibility with temperature. An intermediate time scale internal motion ($\tau_i \approx 0.5$ ns) which is slowed down at 15 °C is observed for Asp5 at 25 °C. Similar internal motion was also observed for Leu6 at 15 °C only. Very large R_{ex} values that decrease with temperature were found for residues 1, 2, and 7.

3.2.4. Temperature Dependence of Order Parameter. Figure 6A shows that the order parameter S^2 decreases with temperature for all residues. In order to estimate T^*, a characteristic temperature for the dynamical process, plots of $(1 - S)$ versus T were drawn (see Figure 7A for residues 3, 5, and 7). Values between 135 and 236 K were obtained (Table 3).

3.2.5. Temperature Dependence of Chemical Exchange. $\ln(R_{ex})$ was plotted against $1/T$ to estimate the apparent activation energy E_a associated with the μs−ms time scale motions (Figure 7B). The linear dependence observed for residues 1, 2, and 7 gave values of 43, 35 ± 10, and 36 ± 2 kJ/mol, respectively (Table 3). For the other residues, the R_{ex} values were relatively small, and no significant variation was observed with temperature.

3.2.6. CPMG Delay Dependence of Chemical Exchange. R_2 experiments were recorded at 35 °C with several CPMG delays: $\tau_{CPMG} = 900$, 380, 120, and 68 μs. Figure 8A displays the difference of R_2 between the longest and the shortest delay. Residues 1, 2, and 7, which had the highest chemical exchange terms, showed large variations, higher than 2 s^{-1}, whereas the others displayed no significant change. Values for R_{ex} were derived using a correlation time of 6.4 ns in the model-free analysis. They were plotted against $1/\tau_{CPMG}$ (Figure 8B), for residues 1, 2, and 7, in order to obtain estimates of the exchange rate k_{ex} through eq 4. The values obtained, around 2×10^5 s^{-1}, are shown in Table 3.

3.3. ^{15}N Relaxation in Other Media. 3.3.1. ^{15}N Relaxation in DPC Micellar Solution. A relaxation study was then performed in DPC micelles to evaluate the influence of the detergent on the dynamic properties. After having assigned ^{1}H and ^{15}N signals (available in Supporting Information) using the standard 2D homonuclear and HSQC experiments, R_1, R_2, and NOE ^{15}N relaxation parameters were measured at 35 °C only,

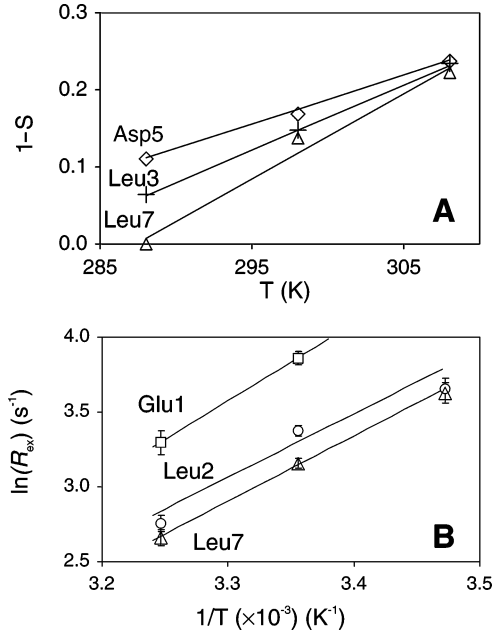

Figure 7. Temperature dependence of dynamical parameters for surfactin in SDS micelles. (A) $1 - S$ versus the temperature is represented for residues 3 (crosses), 5 (diamonds), and 7 (triangles). The slope of the fitted curves enabled to derive the characteristic temperatures T^* reported in Table 3. (B) Arrhenius plots of $\ln(R_{ex})$ versus the inverse of the temperature for residues 1 (squares), 2 (circles), and 7 (triangles) exhibiting significant exchange terms. Apparent activation energies derived from the slope of the graphs are given in Table 3. Two temperatures only could be used for residue 1, since data at 15 °C was missing.

Table 3. Apparent Exchange Rate, Activation Energy, and Characteristic Temperature for Surfactin in SDS Micellar Solution

residue	k_{ex} (ms^{-1})	E_a ($kJ.mol^{-1}$)	T^* (K)
Glu1	203 ± 27	43[a]	182[a]
Leu2	128 ± 31	35 ± 10	228 ± 69
Leu3	-	-	177 ± 12
Val4	-	-	216 ± 93
Asp5	-	-	236 ± 10
Leu6	-	-	228 ± 55
Leu7	195 ± 56	36 ± 2	135 ± 18

[a] The activation energy and characteristic temperature for residue 1 were estimated from the slope of $\ln R_{ex} = f(1/T)$ or $1 - S = f(T)$, respectively, using two points only (at 25 °C and 35 °C).

as extensive signal broadening was already observed at 25 °C. As shown in Figure 9, the profiles are very similar to those obtained in SDS at 25 °C with, however, slightly higher R_1 and NOE values (Table 2). The presence of very large R_2 values for residues 1, 2, and 7 in SDS and DPC media indicate μs−ms time scale chemical exchange around the fatty acid. As shown in Figure 10, reduced spectral density mapping confirms those observations. Indeed, $J(0)$ values in DPC are nearly identical to those in SDS at 25 °C, whereas $J(\omega_N)$ and $\langle J(\omega_H)\rangle$ values are globally intermediate between those at 25 °C and 35 °C in SDS and exhibit the same general pattern along the peptide sequence (Figures 5 and 10). No model-free analysis was performed since the global correlation time could not be reliably inferred from the relaxation data.

3.3.2. ^{15}N Relaxation in DMSO. Both studies in SDS and DPC micelles evidenced chemical exchange around the fatty acid by which the peptide must be anchored into the micelle. In order to determine if this chemical exchange was related to the presence of micelles, relaxation experiments were also

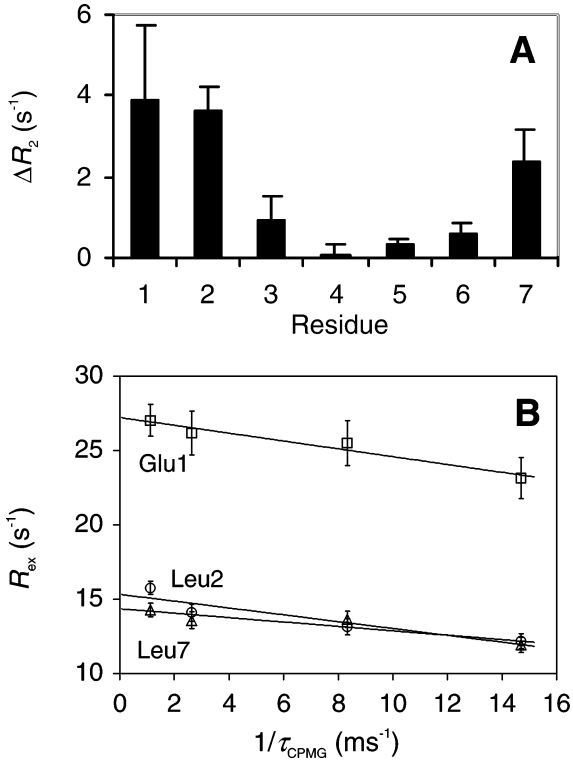

Figure 8. Chemical exchange study by CPMG experiments for surfactin in SDS micelles at 35 °C. (A) Difference in R_2 between the longest CPMG delay (900 μs) and the shortest one (68 μs). (B) R_{ex} plotted against the inverse of the CPMG delay for residues 1 (squares), 2 (circles), and 7 (triangles). The data were fitted to eq 4 to derive the apparent exchange rates k_{ex} reported in Table 3.

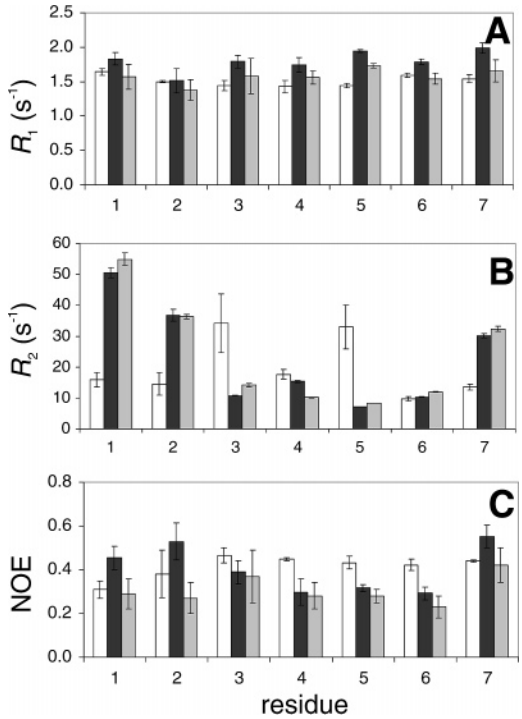

Figure 9. Backbone amide ^{15}N relaxation parameters for surfactin in various media. (A) R_1, (B) R_2, and (C) heteronuclear NOE in DMSO at 25 °C (white boxes), in DPC micelles at 35 °C (black boxes), and in SDS aqueous solution at 25 °C (gray boxes).

carried out in DMSO organic solvent. Proton and ^{15}N assignments in DMSO were performed beforehand at 25 °C and can

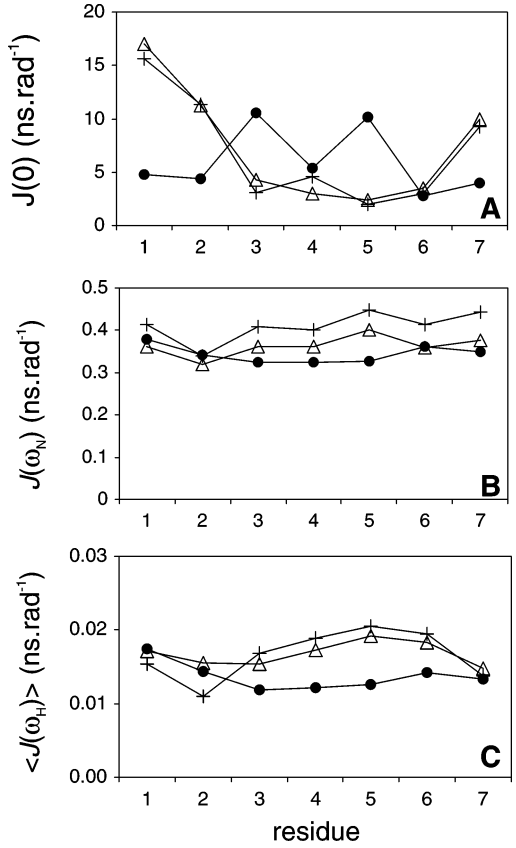

Figure 10. Spectral density function values for surfactin in various media. (A) $J_{eff}(0)$, (B) $J(\omega_N)$, and (C) $\langle J(\omega_H)\rangle$ values were collected in DMSO at 25 °C (filled circles), in DPC micelles at 35 °C (crosses), and in SDS micelles at 25 °C (triangles).

be found in Supporting Information. Figure 9 shows that the R_2 profile in DMSO strikingly differs from that in micellar solution. Here, large R_2 values are not observed for residues 1, 2, and 7 but for residues 3 and 5 instead. Concerning the R_1 and NOE profiles, they do not exhibit significant changes in this organic solvent. The averages for R_1 and R_2 (excluding the values of the residues 3 and 5 containing a large exchange contribution) are close to those in SDS at 25 °C, while that for the NOE is slightly higher (Table 2). The differences in dynamic properties in DMSO are also clearly visible in the reduced spectral density mapping analysis (Figure 10). The difference in $J_{eff}(0)$ is striking, and changes in $J(\omega_N)$ and $\langle J(\omega_H)\rangle$ can also be observed. The $\langle J(\omega_H)\rangle$ frequency values in DMSO at 25 °C are on average lower than those in SDS at the same temperature (Figure 10C).

4. Discussion

4.1. Structure of Surfactin in Aqueous Micellar Medium. In this study, we determined the 3-D structure of surfactin in SDS micellar aqueous solution and found a single family of structures of low energy, whereas two families, *S1* and *S2*, of similar energetic minima were previously obtained in organic solvent.[4] We can therefore hypothesize that SDS micelles stabilize this conformation by a particular solvation. Besides, the presence of two mirror-like conformations in DMSO might originate from the modeling protocol. A similar phenomenon was already observed for other cyclopeptides.[52]

The structure obtained in the SDS membrane-mimicking medium can be superimposed neither with the *S1* nor with the *S2* structure described in the organic solvent. The main H-bonds observed are also different from those present in DMSO.[4] However, the backbone still adopts a saddle-shaped conformation, with the two acidic residues lying on the same side of the molecule (Figure 3B). As far as hydrophobic residues are concerned, they are all exposed toward the opposite side, except for Val4. The surface electrostatic profile shows a negatively charged patch surrounded by a large neutral hydrophobic domain (Figure 3, C and D), which is favorable for auto-association and is consistent with the powerful surfactant properties of this molecule. The slow exchange rate with D_2O observed for the amide protons of Leu3 and Leu7 cannot be explained by the intramolecular H-bond network obtained but might stem from intermolecular H-bonds or a hydrophobic protective environment.

The modeling of surfactin in DPC micelles has been investigated too; however, fewer distance and angle restraints could be obtained from the NMR spectra than were obtained for SDS micelles. The structure was therefore more poorly defined (data not shown). However, the structural features of surfactin in SDS or DPC micelles were found to be globally similar and to differ significantly from those described in DMSO.[4]

4.2. Dynamics of Surfactin in Aqueous SDS Micellar Medium. A model-free analysis of the relaxation parameters was performed at 15, 25, and 35 °C, despite the difficulty to spot, in this very small peptide, residues without chemical exchange terms or active internal motion. These conditions are indeed required to derive the global correlation time that will be used to obtain the different mobility parameters. A correlation time value was determined from the relaxation data at 15 °C, which appeared to be the most reliable data for this approach, as the NOE values observed were not too low and some residues seemed to contain no or very little exchange term. This provided an estimation for τ_c of 10.9 ± 0.1 ns. For the data at 25 and 35 °C, internal motion was obviously apparent for all residues, given the low NOE values. We consequently chose to use the Stokes−Einstein relation to estimate values of τ_c at the two other temperatures, assuming a temperature effect on the viscosity only, and evaluated that $\tau_c = 8.2 \pm 0.1$ ns at 25 °C and 6.4 ± 0.1 ns at 35 °C. Despite the various approximations and assumptions made, reasonable values of τ_c were found. Indeed, they are consistent with those reported in the literature for peptides solubilized in SDS micellar solutions: for example, $\tau_c = 6.6$ ns at 35 °C for the 22-residue motilin,[53] $\tau_c = 7.5$ ns at 37 °C for the 16-residue penetratin,[54] and $\tau_c = 8$ ns at 25 °C for the 30 N-terminal residues of HIV-1 gp41.[18] Finally, the use of the Lipari−Szabo approach is strengthened by the fact that the local mobility parameters derived using these τ_c values seem very plausible, as discussed later, and consistent with those obtained by the spectral density mapping that was not based on any of these assumptions.

The order parameter does not vary much along the peptide sequence (Figure 6A), indicating the same degree of flexibility. Average values are 0.59 ± 0.03, 0.67 ± 0.04, and 0.86 ± 0.10

(52) Volpon, L.; Tsan, P.; Majer, Z.; Vass, E.; Hollósi, M.; Noguéra, V.; Lancelin, J.-M.; Besson, F. *Spectrochim. Acta, Part A Mol. Biomol. Spectrosc.* **2006**, doi:10.1016/j.saa.2006.10.027.
(53) Jarvet, J.; Zdunek, J.; Damberg, P.; Graslund, A. *Biochemistry* **1997**, *36*, 8153−8163.
(54) Andersson, A.; Almqvist, J.; Hagn, F.; Maler, L. *Biochim. Biophys. Acta* **2004**, *1661*, 18−25.

at 35 °C, 25 °C, and 15 °C respectively, indicating that the rigidity of the backbone increases as the temperature is lowered. The slope of $1 - S$ versus T provided an estimation of the characteristic temperature T^*. T^*/T is related to the number of states accessible thermally: the lower T^*/T is, the higher this number is. In their study, Mandel et al.[48] found values around 3 for secondary structures of ribonuclease H, around 1 for loops, and about 0.6 for the C-terminus. In our case, we obtained values of T^* ranging between 135 and 236 K, giving values of T^*/T around 0.45−0.79 at room temperature. The number of thermally accessible states for our cyclopeptide is therefore much higher than for secondary structures and is closer to the case of loops and even unstructured terminal extremities.

Dramatically large R_{ex} were found for residues 1, 2, and 7, indicating μs−ms conformational exchange. To get a closer insight into this chemical exchange, we studied the temperature dependence of R_{ex} and obtained activation energy values of 43, 35 ± 10, and 36 ± 2 kJ/mol, respectively. These values fall within the same range as those determined for some conformational motion in ribonuclease H (20−50 kJ/mol), [48] or ribonuclease A (15−31 kJ/mol),[55] which are intermediate values between activation energies of methyl rotations (∼14 kJ/mol) and ring flips (>57 kJ/mol) for instance. Moreover, we carried out R_2 experiments with various CPMG delays in order to derive an apparent exchange rate k_{ex}. Our results are consistent with the theoretical dependence of R_{ex} against $k_{ex}\tau_{CPMG}$ described by Beeser et al., calculated for a simple two-site exchange model.[56] In this model, R_{ex} is indeed zero for $k_{ex}\tau_{CPMG} \ll 1$, increases with a maximal variation for $k_{ex}\tau_{CPMG} = 1$ and reaches a plateau for $k_{ex}\tau_{CPMG} \gg 1$. We found for surfactin a $k_{ex}\tau_{CPMG} \approx 13-180$, which is effectively in the region where R_{ex} is expected to be observable and to vary with τ_{CPMG} (Figure 8, A and B). The values for k_{ex} are, however, quite high when compared to results obtained for large proteins such as the H80E mutant of bovine neurophysin-I, in which a dimerization-induced conformational change would occur at $k_{ex} = 63-490$ s^{-1} at the hormone binding site.[57] It is also higher than the average value for slow exchanging residues in the active site and the substrate binding site of ribonuclease A ($k_{ex} = 1640$ s^{-1})[55] for the calcium binding site of the synaptotagmin I C2A ($k_{ex} = 2000$ s^{-1})[58] and for the unfolding of the Fyn SH3 domain mutant ($k_{ex} \approx 5000$ s^{-1}).[59] Our results for surfactin ($k_{ex} = 128{,}000-203{,}000$ s^{-1}) are more similar to the large-scale but slow conformational change found around the trypsin binding site of a bovine pancreatic trypsin inhibitor mutant for which the mutation was shown to cause a large thermodynamic destabilization of 5 kcal/mol.[55] The k_{ex} was indeed estimated between 50,000 and 200,000 s^{-1}. Finally, the activation energy obtained for surfactin does not exclude the hypothesis of slow conformational exchange around FA8. It could then account for the structural disorder around FA8 observed in our surfactin model in SDS micelles (Figure 3A), similar to that in some mobile loops in proteins for instance. The exchange rate k_{ex} is however higher than the values reported in folded proteins, and only gets close to those found in a destabilized mutated protein. We then extended this dynamics study to other media to check this hypothesis.

4.3. Comparison of the Dynamics of Surfactin in Various Media. Relaxation studies in DPC micelles allowed evaluation of the influence of the detergent polar head on the dynamic properties. Indeed, DPC forms micelles of similar size to that of SDS micelles but possesses a zwitterionic phosphocholine head instead of a negatively charged sulfate. Besides, while SDS can model the bacterial membranes containing a significant amount of anionic compounds, DPC micelles mimick the mammalian membranes composed of mainly uncharged phosphatidylcholine lipids.[60] Relaxation parameters of surfactin in DPC micelles showed similar main features to those in SDS, i.e., very large R_2 for residues 1, 2, and 7 and rather constant R_1 and NOE values along the sequence. The average values are, however, slightly different from those in SDS at the same temperature, probably due to slightly different overall tumbling properties in this detergent. This shows that changing a sulfate negatively charged head into a zwitterionic phosphocholine does not qualitatively modify the local dynamics, but only quantitatively, as well as the global dynamics. In contrast, changing from a micellar solution into an organic solvent significantly perturbs the local dynamics. Particularly, the large exchange contribution found around the fatty acid is not present in DMSO, which proves that it is related to the micellar environment. In our first hypothesis that the exchange term would reflect a structural disorder in the backbone conformation, this would mean that the intrinsic dynamic properties of surfactin are completely changed from micellar to organic media. This could be possible, as the structure found in SDS or DPC micelles is slightly different from that in DMSO as well. Nevertheless, a second interpretation could also be proposed: the exchange contribution may stem from the interaction of the lipopeptide with the micelle. It might reflect, for instance, motion of surfactin within the micelle or an equilibrium of surfactin between a micelle-bound conformation and a nonbound one. Indeed, the residues around the lipidic tail, by which the lipopeptide must be inserted into the micelle, would then be expected to exhibit the largest exchange term. Moreover, that could explain the rather high k_{ex} exchange rate found for surfactin compared to most values found in literature, which were determined for proteins in non-micellar media. The activation energy for the rotational diffusion of a phospholipid-type spin probe was found to be ∼25 kJ/mol in phosphatidylcholine model membranes,[61] whereas rotation of chloroplast ATP synthase within phospholipid vesicles was found to be ∼32−40 kJ/mol.[62] Consequently, the activation energy of 35−43 kJ/mol estimated for the conformational exchange in surfactin could also be consistent with the hypothesis of such rotational motion within the SDS micelle. However, no other NMR studies of similar systems reporting such large exchange terms are available to assess it. The closest case would be a 50 amino acid protein comprising two α-helices, one amphipathic located on the surface of the micelle and one hydrophobic within the micelle.[63] The motion of the hydrophobic helix was found to

(55) Cole, R.; Loria, J. P. *Biochemistry* **2002**, *41*, 6072−6081.
(56) Beeser, S. A.; Goldenberg, D. P.; Oas, T. G. *J. Mol. Biol.* **1997**, *269*, 154−164.
(57) Naik, M. T.; Lee, H.; Bracken, C.; Breslow, E. *Biochemistry* **2005**, *44*, 11766−11776.
(58) Millet, O.; Bernado, P.; Garcia, J.; Rizo, J.; Pons, M. *FEBS Lett.* **2002**, *516*, 93−96.
(59) Korzhnev, D. M.; Neudecker, P.; Mittermaier, A.; Orekhov, V. Y.; Kay, L. E. *J. Am. Chem. Soc.* **2005**, *127*, 15602−15611.
(60) Khandelia, H.; Kaznessis, Y. N. *Peptides* **2006**, *6*, 1192−1200.
(61) Shin, Y. K.; Freed, J. H. *Biophys J.* **1989**, *55*, 537−550.
(62) Musier-Forsyth, K. M.; Hammes, G. G. *Biochemistry* **1990**, *29*, 3236−3241.
(63) Papavoine C. H.; Christiaans, B. E.; Folmer, R. H.; Konings, R. N.; Hilbers, C. W. *Biochemistry* **1997**, *36*, 4015−4026.

be more restricted and, more importantly, to contain a slow conformational exchange component, which would be in favor of our second hypothesis. However, the opposite case was also observed for phospholamban that also possesses an amphipathic and a transmembrane helix: in this case, slow conformational exchange was found mainly for the amphipathic helix.[64] Their interpretation was that this helix is exposed in the cytoplasm and such dynamic features must be important for biomolecular recognition.

5. Concluding Remarks

In summary, the dynamic properties of surfactin are qualitatively the same in SDS negatively charged micelles and in DPC uncharged micelles and only differ quantitatively. Surprisingly large exchange terms were observed around the fatty acid of surfactin in micellar solution, but not in DMSO. Two interpretations have been proposed and discussed: intrinsic slow conformational exchange in the backbone segment around FA8 or dynamics related to a peptide/micelle interaction. Both phenomena could, in fact, occur at the same time and together explain the results. Last, these structural and dynamic results on surfactin provide both a model of this biosurfactant determined in biomimetic media (which could be used for interaction studies with membranes by computer simulations, for instance) and unusual NMR results of an original lipopeptide/micelle system.

(64) Metcalfe, E. E.; Zamoon, J.; Thomas, D. D.; Veglia, G. *Biophys. J.* **2004**, *87*, 1205−1214.

Abbreviations

FA8, β-amino fatty acid at position 8; CPMG, Carr−Purcell−Meiboom−Gill; DMSO, dimethylsulfoxide; DPC, dodecyl phosphocholine; DQF-COSY, double quantum filtered correlation spectroscopy; FID, free induction decay; H-bond, hydrogen bond; HOHAHA, homonuclear Hartmann−Hann spectroscopy; HSQC, heteronuclear single quantum correlation; NOE, nuclear Overhauser effect; NOESY, nuclear Overhauser effect spectroscopy; R_1, longitudinal relaxation rate; R_2, transverse relaxation rate; SDS, sodium dodecyl sulfate; TOCSY, total correlation spectroscopy; RMSD, root mean square deviation.

Acknowledgment. L.V. was recipient of a PhD fellowship 1998-2001 from the French *Ministère de l'Education Nationale de la Recherche et de la Technologie.* We are grateful to Benoît Rigard for his helpful participation in the experimental work.

Supporting Information Available: ^{15}N and ^{1}H chemical shifts of surfactin in SDS micelles, DPC micelles and in DMSO. This material is available free of charge via the Internet at http://pubs.acs.org.

JA066117Q